

Direct measurements for the fine-structure splitting of S VIII and Cl IXQ. Lu ¹, C. L. Yan ¹, G. Q. Xu ¹, N. Fu ¹, Y. Yang¹, Y. Zou¹, A. V. Volotka ^{2,3},
J. Xiao ^{1,*}, N. Nakamura^{4,†} and R. Hutton¹¹*Shanghai EBIT Laboratory, Key Laboratory of Nuclear Physics and Ion-Beam Application (MOE),
Institute of Modern Physics, Fudan University, Shanghai 200433, China*²*Helmholtz-Institut Jena, D-07743 Jena, Germany*³*GSI Helmholtzzentrum für Schwerionenforschung, D-64291 Darmstadt, Germany*⁴*Institute for Laser Science, The University of Electro-Communications, Chofu, Tokyo 182-8585, Japan*

(Received 12 August 2020; accepted 5 October 2020; published 21 October 2020)

Using electron-beam ion traps (EBITs), we have made direct measurements for the fine-structure splitting $2p^5$ of S VIII and Cl IX, which are important to the test of *ab initio* theory in F-like ions. Their wavelength are redetermined in the laboratory with an accuracy of 23 ppm, i.e., $10\,085.40 \pm 0.23\text{ cm}^{-1}$ for S VIII, where the early value observed in the solar spectrum is questionable, and $13\,643.39 \pm 0.32\text{ cm}^{-1}$ for Cl IX, where only indirect measurements had been performed. High-precision calculations, including *ab initio* treatment of QED effects, are accomplished for $10 \leq Z \leq 18$ and compared with the experimental results. Good agreement is found between our experimental and theoretical values of the fine-structure energy among these ions except for Al V, which calls for further investigations. Besides, we have succeeded in pushing EBIT operation towards the infrared spectral region relevant to astrophysics.

DOI: [10.1103/PhysRevA.102.042817](https://doi.org/10.1103/PhysRevA.102.042817)**I. INTRODUCTION**

To calculate transition energies for highly charged ions with high accuracy, one should include sufficient electron correlation effects, and appropriate corrections due to relativistic as well as quantum electrodynamic (QED) effects. Recently, Li *et al.* [1] demonstrated that the ground-term transition energies of F-like ions, i.e., $2p^5\ ^2P_{3/2} - ^2P_{1/2}$, can be evaluated theoretically with high accuracy since the correlations' effects are strongly diminished due to the Layzer quenching effect [2,3]. Proper control of the correlations allows one to access typically small quantum electrodynamic (QED) effects. Initially, Li *et al.* [1] employed three different approximate techniques for calculating QED corrections, namely (1) “GRASP2K,” the standard approach in GRASP2K code [4], (2) “Welton,” based on Welton’s concept of electron self-energy [5,6], and (3) “Model QED,” Shabaev’s model Lamb-shift operator [7,8]. It was found that the first two methods give very similar results for all ions considered, but the latter predicts universally more significant values for the QED effects. To some extent, the spread of the obtained results represents the uncertainty of the calculations. This statement is also confirmed by the available experimental values that lie between these two results of QED treatment, except for two regions, very high- Z and very low- Z ions. The case of high- Z discrepancy was explained by Volotka *et al.* [9] with *ab initio* QED calculation, which includes all first-order and many-electron second-order QED effects. Later, Shabaev *et al.* [10]

modified the model QED operator and their results started to agree with the experimental QED contributions in case of F-like uranium. However, the discrepancy for low- Z left. As can be seen from Fig. 2 in Ref. [1], the comparison between experiment and theory for Na III and Mg IV implies a trend where the experimental values approach the GRASP2K (or Welton) results, and for Al V goes below GRASP2K leaving the spread between GRASP2K and model QED curves, while for Ar X the experimental value comes back into the spread and agrees with rigorous computation [9]. It should be stressed that only wavelengths from direct measurements of the $M1$ transitions are adopted and compared with theoretical calculations. Note that the Ne II data are from infrared Fourier transform spectroscopy [11] and the Ar X data are from electron-beam ion trap (EBIT) spectroscopy [12]. The data points for Na III, Mg IV, and Al V [13] are all from astrophysical measurements. The question of how this transition develops from Si VI to Cl IX becomes important, so accurate experimental measurements for the fine-structure splitting of these ions are urgently required.

So far, the ground configuration interval of S VIII was experimentally measured as $10\,080\text{ cm}^{-1}$ by Robinson [14]. Note that this was not a direct measurement, but a separation of two extreme ultraviolet (EUV) lines ($503\,652$ and $493\,571\text{ cm}^{-1}$). Kissell *et al.* [15] found $10\,087\text{ cm}^{-1}$ (9913.7 \AA , in vacuum) as a direct measurement of the $M1$ transition observed in the solar spectrum, where the wavelength uncertainty was 1 cm^{-1} . Nevertheless, Jefferies listed this observation as needing confirmation [16,17]. For the measurement of the ground term transition of Cl IX, Kaufman *et al.* [18] produced a laser plasma and this transition was indirectly measured as $13\,631 \pm 40\text{ cm}^{-1}$. This value is close

*Corresponding author: xiao_jun@fudan.edu.cn

†Corresponding author: n_nakamu@ils.uec.ac.jp

to that reported by Jupén [19] as $13\,629\text{ cm}^{-1}$, which was remeasured from unpublished recordings by Edlén. However, according to the publications by Edlén himself [20–23] and Ref. [15], this experimentally measured splitting for Cl IX is $13\,641 \pm 5\text{ cm}^{-1}$, which deviates 12 cm^{-1} from Ref. [19]. In brief, these values of all the available experimental data for the fine-structure splitting of S VIII and Cl IX show a great discrepancy, while the error bar of those either remains unknown or relatively big. Thus, remeasurements for the fine-structure splitting of S VIII and Cl IX are necessary.

Apart from the aid to the test of *ab initio* theory, the F-like ions are also of great interest in the study of many solar coronal lines in the laboratory and astrophysical plasma diagnostics [24–27]. For example, many problems concerned with solar physics remain unsolved, mostly due to the complexity of solar magnetism [28,29], and *M1* transitions of abundant coronal ions have been used for the measurement of the coronal magnetic fields [30]. Note that S and Cl are important elements in the cosmos [31], and the ground term transitions in F-like ions with the upper level $J = 1/2$ are unpolarizable. Thus, the F-like ions of S and Cl are of potential interest for the calibration of astronomical instruments, such as the 4 m, Daniel K. Inouye Solar Telescope (DKIST, formerly ATST) [28,29,32].

An electron-beam ion trap (EBIT) employs a monoenergetic and energy-adjustable electron beam to ionize trapped ions, which has been proved to be one of the most versatile light sources for spectroscopic studies. Many works on the ground-state fine-structure splitting of F-like ions have been accomplished with EBIT devices [12,33–36]. Furthermore, EBITs have also been successfully utilized for astrophysics-study purposes [37–40]. However, up to now EBITs have not been used in the infrared region probably because of concern about blackbody radiation from the electron gun overpowering the weak signal.

To provide credible data for the fine-structure splitting of S VIII and Cl IX with high accuracy for the test of *ab initio* theory, as well as to push EBIT operation towards the infrared spectral region relevant to astrophysics, we have performed two measurements with EBIT devices. Based on ongoing collaboration, the fine-structure splitting of S VIII is measured on the CoBIT in Tokyo [41], while that of Cl IX is accomplished on the SH-HtscEBIT in Shanghai [42,43]. Laboratory measurements for the fine-structure splitting of S VIII and Cl IX are presented. QED corrections with *ab initio* calculations for $10 \leq Z \leq 18$ are also accomplished and compared with our experimental results.

II. EXPERIMENTS FOR S VIII AND Cl IX

A. Experiment for S VIII

Our measurements for the fine-structure splitting of S VIII were conducted using CoBIT [41]. CoBIT mainly consists of an electron gun, an ion trap (drift tube), an electron collector, a superconducting coil, and a liquid-nitrogen tank. A high critical temperature superconducting Helmholtz-like coil, which can be used at the liquid-nitrogen temperature, is mounted around the drift tube. An electron beam emitted from the electron gun is accelerated toward the drift tube while being

TABLE I. Wavelengths (in vacuum) of the reference lines [44].

Element	Wavelength (nm)
Ne	966.80709
Ar	966.0435, 978.7186
Xe	968.798, 972.083, 980.2384, 992.5919, 1011.011
Hg	1014.253

compressed by a magnetic field produced by the superconducting coil. After passing through the drift tube, the electron beam is collected by the electron collector. In order to produce highly charged sulfur ions, SF₆ gas was injected into CoBIT through a gas injection system. The ion trap was dumped with a frequency of 0.5 Hz for preventing impurity heavy ions from being accumulated in the trap.

Emission from the trapped sulfur ions was observed with a commercial Czerny-Turner type of visible spectrometer (Jobin Yvon HR-320) with a 1200-gr/mm grating blazed at 400 nm (Jobin Yvon 51006). A convex lens was used to focus the emission from the trap on the entrance slit of the spectrometer. The diffracted light was detected with a Peltier-cooled back illuminated charge-coupled device (CCD) (Andor iDus 416) operated at $-70\text{ }^\circ\text{C}$.

The wavelength scale was calibrated using emission lines from Ne, Ar, Xe, and Hg lamps placed outside CoBIT. The wavelengths [44] of the reference lines used in the present study are listed in Table I. The conversion function from the CCD pixel number to the wavelength was obtained by fitting a cubic function to the peak positions of the reference lines. A 1-h accumulation was repeated several times for the observation of the sulfur line. The observation of the reference lamps was done in between sulfur observations.

Emission from the trapped sulfur ions in the EUV range was also monitored by a grazing incidence flat field grating spectrometer [45] with an aberration corrected concave grating (Hitachi 001–0660) and a Peltier-cooled back illuminated CCD (Princeton PIXIS-XO 400B) cooled at $-70\text{ }^\circ\text{C}$.

Figure 1 shows the experimental spectrum obtained with an electron beam of 380 eV and 10 mA. At the same time, the $2s^22p^5-2s^12p^6$ transition at 19.86 nm was observed with the EUV spectrometer. It was confirmed that the line indicated by the blue arrow in Fig. 1 and the EUV transition at 19.86 nm showed the same dependence on the electron energy. From the energy dependence and the comparison with the known energy interval of the $J = 3/2 - 1/2$ fine-structure splitting of $2p^5$ ($10\,085\text{ cm}^{-1}$ [44], which was obtained as an average of the two semiempirically estimated values [21,46]), we identified the line indicated by the blue arrow in Fig. 1 to be the magnetic dipole transition between the $J = 3/2 - 1/2$ fine-structure splitting of $2p^5$ in S VIII. The wavelength scale for this spectrum was calibrated with eight lines of Ne, Ar, and Xe listed in Table I because the Hg line was out of the observed wavelength range. The peak center obtained by unweighted fitting of a Gaussian function to the experimental data is 991.530 nm (in vacuum) with a fitting error of 0.005 nm. The wavelength value can be converted to $10\,085.42 \pm 0.05\text{ cm}^{-1}$ as the $J = 3/2 - 1/2$ fine-structure splitting of $2p^5$.

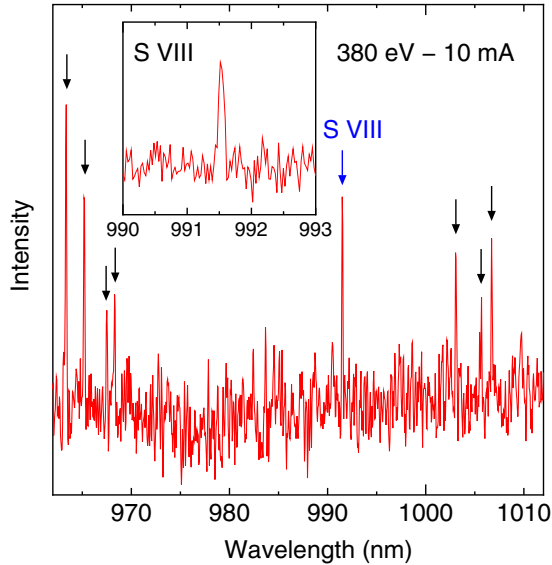


FIG. 1. Infrared spectrum observed with CoBIT. The electron-beam energy and current were 380 eV and 10 mA, respectively. The line indicated by the blue arrow is the magnetic dipole transition in S VIII. The other lines indicated by the black arrows are considered to be S II lines (some of them are the second-order refraction of visible transitions at around 500 nm). The inset shows the closeup view of the S VIII transition.

In order to deduce the wavelength value in vacuum, the wavelength calibration was done using the reference wavelength values in vacuum as listed in Table I despite that the spectrometer was operated in air. Calibration with the reference wavelength values in air was also made, and the air wavelength of 991.258 nm was obtained. By using a refractive index value of 1.000 274 [47], the air value can be converted to the vacuum value of 991.530 nm, which is consistent with the value obtained by the analysis with the reference wavelength values in vacuum. This confirms that the wavelength dependence of the refractive index does not affect the wavelength determination using the wavelength values in vacuum.

Since the grating used in the present observation was not appropriate for the infrared range and there was strong infrared background arising from the electron gun cathode, the observation required a long accumulation time. The spectrum shown in Fig. 1 is the sum of five accumulations (5 h). The mechanical and thermal drifts $\Delta\lambda_{\text{drift}}$ during the long accumulation time can be estimated from the lamp spectra obtained in between observations of the sulfur data. Although the origin of the drift is not clear, the drift was confirmed to be about ± 0.2 pixel, which corresponds to ± 0.005 nm.

Similar measurements were performed two more times with different angles of the diffraction grating (and thus with the different positions on the CCD). The second measurement with four accumulations (4 h), which was calibrated with seven lines (Ne, Ar, and Xe lines except for the 1011-nm line), gave 991.545 nm with a fitting error of 0.005 nm. The drifting was confirmed to be within 0.008 nm. The third measurement with four accumulations (4 h), which was calibrated with eight lines (Ar, Xe, and Hg lines), gave 991.530 nm with

TABLE II. Experimentally obtained wavelength (in vacuum) for the magnetic dipole line in S VIII and the line observed at 1003 nm, which is preliminarily assigned as the second-order refraction of visible transition in S II. The experimental wavelength and the fitting error are listed as $\lambda \pm \Delta\lambda_{\text{fit}}$, whereas $\Delta\lambda_{\text{drift}}$ represents a systematic error arising from drifting (see text for details). All values are in nm.

Experiment number	S VIII	1003-nm line	$\Delta\lambda_{\text{drift}}$
1	991.530 ± 0.005	1003.086 ± 0.008	0.005
2	991.545 ± 0.005		0.008
3	991.530 ± 0.005	1003.065 ± 0.006	0.005
Weighted average	991.532	1003.073	

a fitting error of 0.005 nm. The drifting was confirmed to be within 0.005 nm. Results of the three measurements are summarized in Table II. It is confirmed that the reproducibility is within 0.015 nm. Since the fitting error $\Delta\lambda_{\text{fit}}$ in the three measurements was the same, the final value was obtained by the average weighted by $1/\Delta\lambda_{\text{drift}}^2$ to be 991.532 nm.

The reproducibility of the wavelength value was also tested by another line observed at the same time. Table II also shows the experimental wavelength of the line observed at 1003 nm, which is the closest one from the S VIII line. The values obtained in experiments 1 and 3 are shown because we could not observe any line other than the S VIII line in experiment 2 although we do not know why. As seen in the table, the difference between two measurements in wavelength in this line is 0.021 nm, and the average weighted by the fitting error is obtained to be 1003.073 nm. Although we are not sure, this line can be assigned to the second-order refraction of the 501.5468-nm line in S II [44]. If it does, the wavelength should be 1003.094 nm (doubles 501.547 nm), which differs from the experimentally obtained value by 0.020 nm. We consider this deviation, which corresponds to about 3/4 of the dispersion per pixel (0.026 nm/pixel), as a systematic error in the present measurement, which could arise from drifting, calibration, background structure, etc.

As written above, the reference lamps were placed outside CoBIT, which may cause a systematic uncertainty due to a difference in the source position. This systematic uncertainty was tested by observing the same 996-nm line of Ar I emitted from CoBIT and a lamp. The CoBIT spectrum was obtained by injecting Ar gas until the pressure of the CoBIT chamber reached about 7.5×10^{-9} Torr, which is much higher than the pressure of the normal condition where highly charged Ar ions are produced. The electron energy and current were 150 eV and 10 mA, respectively, with 10 Hz dumping of ions. The lamp emission and the CoBIT emission were measured alternately, and the peak position for the CoBIT emission and the lamp emission was confirmed to be consistent within ± 0.2 pixel, which corresponds to ± 0.005 nm. We consider this contribution is also included in the estimated systematic error 0.020 nm.

The fitting error listed in Table II can be regarded as a statistical error. Thus the final statistical error for the averaged wavelength should be less than ± 0.005 nm, such as ± 0.003 nm. The total error in the present measurement is

thus estimated to be ± 0.023 nm as a linear sum of the statistical and the systematic errors. Consequently, $10\,085.40 \pm 0.23$ cm^{-1} is obtained for the $J = 3/2 - 1/2$ fine-structure splitting of $2p^5$ in S VIII in the present study.

B. Experiment for Cl IX

Our measurements for the fine-structure splitting of Cl IX were conducted using the SH-HtscEBIT [42,43]. The electron beam is emitted from a LaB6 cathode and compressed to 150 μm by a magnetic field (0.2 T) created by liquid-nitrogen temperature superconducting coils. The electron-beam energy of this EBIT can be varied from 30 to 4000 eV, and it is therefore able to create lowly charged ions. The background vacuum pressure in the trap center is estimated to be lower than 1.0×10^{-9} Torr, which makes it possible to produce targeted ions mainly through electron collisional ionization with negligible influence from charge exchange. Basically each new charge state is formed at the ionization energy of the previous one, giving an important aid in spectral line identification.

The chlorine ions used in the present work were obtained by continuously injecting CCl_4 gas, which has a very low volatile point at atmospheric pressure. Once the CCl_4 molecules entered the region of central drift tube, they were quickly destroyed. Monoenergetic beam electrons collided with injected atoms to form a thin plasma, and the Cl atoms were ionized in further collisions with beam electrons accelerated by the potential difference between the central drift tube and cathode. Once the ions were formed, they were consequently trapped in the radial direction by the space charge of the electron beam and the magnetic field of the EBIT, and longitudinally by the voltage applied to the EBIT central drift tubes (100 V). The final Cl charge state distribution depended on a number of parameters, e.g., the electron-beam energy, current density, and injection rate, but also on the balance of processes, e.g., ionization, recombination, and charge exchange. Excited ions, some of which decayed through emitting photons, were produced and confined in the central drift tube region.

A high-resolution grazing-incidence flat-field spectrometer which covers the range of 1–50 nm was utilized to record extreme ultraviolet spectra. This spectrometer could reach a resolving power above 800 according to our previous experiments [48,49]. A 450-nm-thick aluminum foil was used and mounted on the window of the miniature ultrahigh vacuum gate valve between the SH-HtscEBIT and the spectrometer to block the visible and infrared light from hot cathode. Because of aluminum absorption edge, only EUV radiation longer than 17.1 nm can pass through this aluminum foil. For the present experiment, a Hitachi varied-line-spacing (VLS) grating (1200 L/mm, part number 001-0659) was used, and an Andor CCD camera (model number DO936N-00W-#BN) was placed at different positions to record different wavelength regions.

For visible spectra, the light was viewed and analyzed by a Czerny-Turner spectrometer from Andor (Sr-303i), which approximately covers the range of 200–800 nm. A biconvex lens of $f = 150$ mm was placed between the window of our EBIT and entrance slit of the spectrometer (30 μm) to obtain

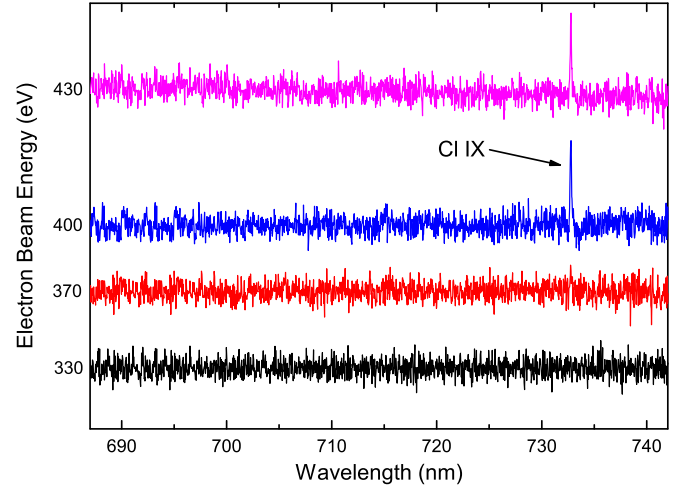


FIG. 2. Spectra of chlorine obtained by SH-HtscEBIT at nominal electron beam energy of 330, 370, 400, and 430 eV in the range 687–742 nm. Line is the $M1$ transition between the fine-structure levels in the $2s^2 2p^5 \ ^2P$ ground term of Cl IX.

a larger collection solid angle. Light from the center of the drift tube was then dispersed by a 1200-L/mm grating blazed at 500 nm and finally detected by a charge-coupled device (Andor DU971P-UVB).

Spectra from Cl IX ions in the visible range 687–742 nm, which were obtained at the nominal electron beam energies of 330, 370, 400, and 430 eV, are shown in Fig. 2. Accumulation time of each spectrum was 2 h. As can be seen from Fig. 2, a line at 732.744 nm emerges when the nominal electron beam energy reaches 370 eV, which just exceeds the ionization energy of Cl VIII, indicating that this line comes from Cl IX. The intensity of this line strongly increases when the electron beam energy is tuned to 400 eV.

To verify the source of this line, the EUV spectra ranging 17–26 nm were also obtained simultaneously. The intensity of line at 18.033 ± 0.034 and 18.494 ± 0.038 nm show the same dependence on electron-beam energy as the visible line at 732.744 nm, making clear they come from the same charge-state ions. According to the NIST database [44], these two EUV lines come from the $E1$ transition $2s^1 2p^6 \ ^6S_{1/2} - 2s^2 2p^5 \ ^2P_{3/2}$ and $2s^1 2p^6 \ ^6S_{1/2} - 2s^2 2p^5 \ ^2P_{1/2}$ respectively, which certifies that the line at 732.744 nm comes from the $M1$ transition $2s^2 2p^5 \ ^2P_{3/2} - 2s^2 2p^5 \ ^2P_{1/2}$.

To improve the signal-to-noise ratio, the accumulation time of our observation for Cl IX spectrum was totally 8 h at the nominal electron-beam energies of 400 eV. The wavelength calibration of this range was accomplished by using external Ne and Ar lamps. According to our calibration results, the wavelength uncertainty for the line at 732.744 nm was 0.017 nm. Note that this uncertainty includes fitting uncertainty as well as dispersion function uncertainty. The systematic uncertainty caused by the difference in positions between the trapped ions and the reference lamps should be taken into account. As shown in Table III, by measuring Ar XI transition $2s^2 2p^4 \ ^3P_2 - ^3P_1$ in the same measurement wave band of the interested Cl IX spectra, and then comparing the wavelength of corresponding line according to NIST database

TABLE III. Comparison of our measured wavelength (nm) for Ar XI and Ar X with NIST [12,44].

Ion	Transition	This work	NIST
Ar XI	$2s^2 2p^4 \ ^3P_2 - ^3P_1$	691.675 ± 0.014	691.6878 ± 0.0012
Ar X	$2s^2 2p^5 \ ^2P_{3/2} - ^2P_{1/2}$	553.310 ± 0.012	553.3265 ± 0.0002

[12,44], this deviation was determined as -0.013 nm. In the same way, the wavelength deviation of Ar X transition $2s^2 2p^5 \ ^2P_{3/2} - ^2P_{1/2}$ was determined as -0.016 nm though the measurement wave band was changed. Considering the spectrometers leading to the nonlinear distribution of actual wavelength, this deviation was finally estimated as -0.013 ± 0.004 nm. Thus, the wavelength of the fine-structure splitting of Cl IX is corrected to 732.757 ± 0.017 nm. The temperature in our laboratory was well stabilized and kept to 20 ± 0.5 °C to eliminate the time-dependent expansion caused by temperature fluctuations. Furthermore, the EBIT, the lens, and the spectrometer would not move since the vibrations caused by the experimental equipment were very weak. Therefore, systematic uncertainty was dominated by the difference in the source positions while thermal and mechanical drifts could be neglected. Consequently, we determine the wave number for the magnetic dipole line in Cl IX as $13\,643.39 \pm 0.32$ cm⁻¹.

III. DISCUSSION

Before proceeding to a detailed comparison of obtained results with previous measurements and calculations, let us briefly discuss the theoretical evaluations performed in the present work. In order to calculate the transition energy $^2P_{3/2} - ^2P_{1/2}$ precisely, one has to consider different corrections to the leading Dirac-Hartree-Fock value. Typically, we refer to these corrections as correlation, Breit [including the Breit(0), frequency-independent Breit interaction, and the Breit(w), frequency-dependent transverse photon exchange], and QED effects [including the one-electron and screened self-energy (SE) and vacuum polarization (VP) diagrams]. As can be seen from Fig. 1 in Ref. [1] and Ref. [50], Breit(0) is the largest correction for all ions. The correlation is the second largest contribution for $Z < 20$, while its relative contribution decreases fast with Z . The Breit(w) contribution in low Z is relatively small compared with other effects.

Thus, the dominant corrections in low Z are Breit(0) and correlation. State-of-the-art calculations of the correlation and Breit corrections for F-like ions were done by Li *et al.* [1]. Consequently, the only correction left is the QED effect. In Ref. [1], the QED effects were first calculated within approximate methods: the method implemented in GRASP2K [4], the Welton treatment of the self-energy [5,6], and the model QED approach [7,8]. Later, the rigorous QED computations were performed by Volotka *et al.* [9] for $Z \geq 18$. Moreover, recently, Shabaev *et al.* [10] reexamined the model QED operator and reached an agreement with the rigorous calculation. Here, we extend the rigorous QED calculations for $Z \leq 18$, as shown in Table IV. The computations are based on the QED perturbation theory in the extended Furry picture. The first-order and second-order many-electron radiative QED corrections are rigorously evaluated. We do not provide all the details of the computations since they are essentially similar to those performed in Ref. [9]. The uncertainty due to the higher-order screened diagrams is estimated to be $(\alpha/8\pi)(\alpha Z)^4/Z^2$ multiplied by a factor of 2.5. In order to reduce this uncertainty, we plan to merge the rigorous QED computations with an approximate treatment. In particular, the third- and higher-order screened radiative corrections extracted from an approximate method can be added to the rigorously evaluated first- and second-order results. These merging calculations are currently underway and will be published elsewhere. However, based on the relative values of the higher-order contributions, we can complement our previous uncertainty analysis, which was based on the comparison of the results obtained with different starting potentials. Although we do not add any additional higher-order correction to the previously published value for Ar, we reduce the uncertainty compared to Ref. [9] by a factor of 2.

In Table IV, we add the results of our direct measurements for S VIII and Cl IX to Ne II [11], Na III, Mg IV, Al V [13], and Ar X [12]. Non-QED values are deduced from theoretical values without QED corrections from Refs. [1,50,51]. It is rather difficult to estimate an uncertainty of the non-QED values since such an estimation is usually based on a comparison with experimental values. For such a comparison, we have to know the QED corrections with better accuracy. However, since the correlation for the considering case can be kept well under control, we assume, here, that the uncertainty of the non-QED values is smaller than the uncertainty of QED contributions. QED corrections (experiment, GRASP2K, Welton,

TABLE IV. Comparison of our QED radiative corrections for $10 \leq Z \leq 18$ with other available values. See the text. All values are in cm⁻¹. The notation for experimental values, e.g., 780.4240(11), implies 780.4240 ± 0.0011 .

Z	Experiment	Non-QED	QED				
			Expt.	This work	GRASP2K	Welton	Model QED
10	780.4240(11)	778.67	1.75	2.4(0.9)	1.78	1.77	2.76
11	1366.5(2)	1363.34	3.2(2)	4.0(1.0)	3.10	3.09	4.63
12	2228.8(1)	2223.74	5.1(1)	6.4(1.2)	5.02	5.01	7.26
13	3442.1(4)	3434.95	7.2(4)	9.5(1.5)	7.71	7.69	10.85
16	10 085.40(23)	10 061.40	24.00(23)	26.2(2.3)	22.26	22.22	29.47
17	13 643.39(32)	13 610.62	32.77(32)	34.8(2.5)	29.96	29.91	39.04
18	18 067.494(7)	18 024.76	42.73(1)	44.4(2.8)	39.46	39.26	50.59

TABLE V. Comparison of experimental and theoretical results of fine-structure splitting of S VIII.

Name	Year	Type	Wave number (cm ⁻¹)
This work	2020	Expt.	10 085.40 ± 0.23
Kissell [15]	1965	Expt. ^a	10 087 ± 1
Robinson [14]	1937	Expt. ^b	10 080
NIST [44]		Theor.	10 085
CHIANTI [57]		Theor. ^c	10 083.98
This work	2020	Theor.	10 087.6 ± 2.3
Li [1,50,51]	2018	Theor. ^d	10 083.66 (10 090.95)
Jönsson [54]	2013	Theor.	10 084.5
Pagan [55]	2011	Theor.	10 087
Bengtsson [56]	1993	Theor.	10 087
Martin [16]	1990	Theor.	10 085
Hata [53]	1983	Theor.	10 081.3
Edlén [21]	1983	Theor.	10 084
Kim [52]	1982	Theor.	10 081 ± 5
Curtis [46]	1982	Theor.	10 086

^aObtained from solar spectrum, but this result is questionable; see the text.

^bIndirect measurements; see the text.

^cTheoretical line given by CHIANTI, Version 7.0 [57].

^dQED effects evaluated with GRASP2K and model QED (value in brackets) by Li *et al.* [1,50,51].

and model QED) are obtained as the difference between the corresponding results (experiment, and theoretical values for GRASP2K, Welton, and model QED from Refs. [1,50,51]) and non-QED values.

We merge our QED radiative corrections for $10 \leq Z \leq 18$ with non-QED values from the GRASP2K results of Li *et al.* [1]. Our direct measurements and theoretical calculations of the fine-structure splitting of S VIII and Cl IX, as well as other experimental and theoretical results given by previous research, are listed in Tables V and VI respectively. As can be seen from Table V, the ground term interval given by Robinson [14] deviates 7 cm⁻¹ from that given by Kissell [15], which has exceeded the error bar given by Kissell. It should be noticed that the former value was obtained from the separation of two EUV lines, while the latter one was observed from the solar spectrum, which is pointed out as needing confirmation by Jefferies [16,17]. Our value is in the middle of the numbers provided by them, and a wavelength measurement accuracy of 22.8 ppm is achieved. The theoretical values are dispersed between 10 081 cm⁻¹ and 10 091 cm⁻¹. Most of the *ab initio* theoretical results (Kim and Huang [52], Hata *et al.* [53], Jönsson *et al.* [54], Li *et al.* [1]) were obtained with the help of the multiconfigurational Dirac-Fock method. Some of the values also include the semiempirical corrections (Curtis and Ramanujam [46], Pagan *et al.* [55], Bengtsson *et al.* [56]). The QED effects were previously estimated either by the approximate potentials or by hydrogenic results. For the values of Li *et al.* [1], we present two results: one with the QED correction calculated with the GRASP2K and another with the model QED approach (value in brackets). Both of our values, theoretical and experimental, are close to other results and in good agreement with each other.

TABLE VI. Comparison of experimental and theoretical results of fine-structure splitting of Cl IX.

Name	Year	Type	Wave number (cm ⁻¹)
This work	2020	Expt.	13 643.39 ± 0.32
Jupén (Edlén) [19]	1985	Expt. ^a	13 629
Kaufman [18]	1982	Expt. ^b	13 631 ± 40
Edlén [20–23]	1977	Expt. ^c	13 641.1 ± 5
NIST [44]		Theor.	13 629
This work	2020	Theor.	13 645.4 ± 2.5
Li [1,50,51]	2018	Theor. ^d	13 640.58 (13 649.76)
Jönsson [54]	2013	Theor.	13 641.64
Edlén [21]	1983	Theor.	13 640
Hata [53]	1983	Theor.	13 638.9
Curtis [46]	1982	Theor.	13 644
Edlén [20]	1982	Theor.	13 641
Kim [52]	1982	Theor.	13 638 ± 5
Edlén [23]	1977	Theor.	13 642.1

^aThis value was reported by Jupén, but the indirect measurements were accomplished by Edlén.

^bIndirect measurements; see the text.

^cThis value was reported by Edlén himself, which deviated a lot from that reported by Jupén.

^dQED effects evaluated with GRASP2K and model QED (value in brackets) by Li *et al.* [1,50,51].

For the ground term interval of Cl IX, the indirectly measured results given by Edlén in different publications exhibit two versions [19–23], i.e., 13 629 cm⁻¹ and 13 641 cm⁻¹, as can be seen from Table VI. This big discrepancy could be quite puzzling, and we are not able to explain it at present. This splitting reported by Kaufman [18] is 13 631 cm⁻¹, which is close to one of Edlén's results [19]. However, the error bar of Kaufman's results has reached up to 40 cm⁻¹. It is easy to understand this large uncertainty, since it also comes from the separation of two levels, both of which gave an uncertainty of 20 cm⁻¹. Our directly measured value, 13 643.39 ± 0.32 cm⁻¹, is close to one of the values given by Edlén [20–23]. As in the case of S VIII, the theoretical spread is rather narrow, ranging from 13 638 cm⁻¹ to 13 650 cm⁻¹ and thus it covers only 9×10^{-4} in relative units. The reason for this is still the same: the transition energy is only slightly sensitive to the correlation effects. Thus, the difference between theoretical values is due to the slight variation in accounting for correlation and due to the treatment of QED effects. Regarding QED, the previous works were mainly based on their approximate treatments. The rigorous evaluation of QED corrections allows us to keep it under control and assign an uncertainty to our theoretical value. Comparing our experimental and theoretical values we find a good agreement as well as with other theoretical results.

Coming back now to a comparison of the experimental and theoretical results for the whole low-*Z* isoelectronic sequence, we present in Fig. 3 available values. For theoretical data, we show the results of Li *et al.* [1] obtained within GRASP2K and model QED approaches together with the rigorous QED calculations [9] extended here also for $Z \leq 18$. As can be seen from the figure, their mutual location stays the same for different ions, i.e., the rigorous QED result lies between

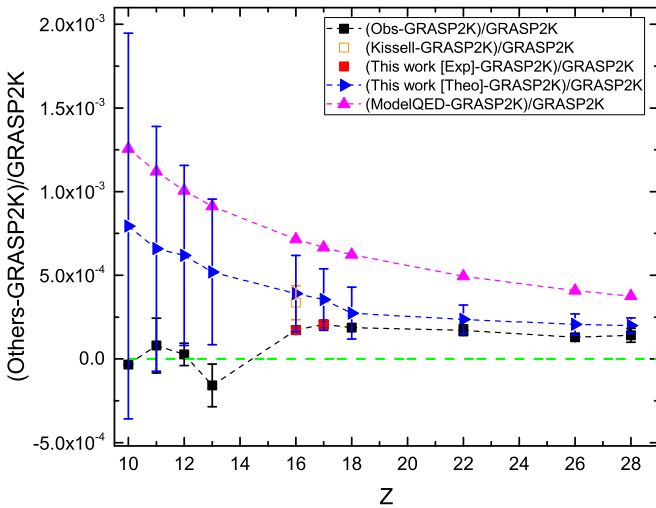


FIG. 3. Comparison of the fine-structure energy splitting of $2p^5\ ^2P$ for $10 \leq Z \leq 28$ from the GRASP2K calculations with the result of model QED calculations (magenta \blacktriangle) and also with the direct observations (black \blacksquare). The Welton results given by Li *et al.* [1] are removed since they are almost the same as GRASP2K. Note that our direct measurements for the fine-structure splitting of S VIII and Cl IX are added to this picture (red \blacksquare) based on the original data presented in Li *et al.* [1]. Direct observations from solar spectrum by Kissell for S VIII (brown \square) are also added, while the results from indirect measurements are abandoned. Our rigorous QED radiative correction calculations combined with non-QED GRASP2K result of Li *et al.* [1] are added as well (blue \blacktriangleright).

GRASP2K and model QED calculations. All the theoretical calculations approach each other with an increase of Z . Thus, different treatments of the QED corrections start to be more precise for heavier ions. As for the experimental results, we display the data for Ne II [11], Na III, Mg IV, Al V [13], Ar X [12], Ti XIV, Fe XVIII, Ni XX [58] from previous measurements together with our results for S VIII and Cl IX. As can be seen from Fig. 3, the experimental values from direct measurements for the fine-structure splitting of S VIII and Cl IX are found between GRASP2K and model QED calculations. At

the same time, they are within the error bar of our theoretical predictions. The theoretical (this work) and experimental data points from S VIII to Ni XX exhibit a trend that they are closer to each other with increasing Z . If we now draw a line connecting the Ne II and Ar X experimental results, we observe that all experimental data in between can be nicely found on this line except for the Al V point. Moreover, the Al V is the only ion remaining, where our rigorous calculations disagree with the experiment.

IV. CONCLUSION

In conclusion, we present direct measurements for the ground term transition $2p^5\ ^2P_{3/2-2}P_{1/2}$ for S VIII and Cl IX. We also extend *ab initio* QED calculations for $10 \leq Z \leq 18$ in F-like ions. Our experimental values are direct wavelength measurements for S VIII and Cl IX in the laboratory. A spectral line near $1\ \mu\text{m}$ is observed within EBIT devices, which extends EBIT spectroscopy in assisting astrophysical research from x-ray, extreme ultraviolet, visible, and to the infrared region. Discrepancies between experimental and theoretical calculations for the fine-structure energy splitting of $2p^5\ ^2P$ for $10 \leq Z \leq 18$ shown by Li *et al.* [1] are solved after our rigorous radiative QED corrections. Comparing the whole low- Z isoelectronic sequence, we observe everywhere an agreement, and it is further improving with an increase of Z . However, there is one exception of the Al V result, which does not match our theoretical values. We call for more experimental work on the direct measurements for the fine-structure splitting $2p^5$ of Al V, Si VI, and P VII, and thus further investigate the low- Z trend in F-like ions.

ACKNOWLEDGMENTS

We acknowledge Dr. M. Li for providing her Ph.D. thesis, Dr. W. Li for useful suggestions, and Dr. R. Si for her help. One of the authors, Q.L., thanks A. Kramida (NIST) for helpful discussions on the fine-structure splitting energy for Cl IX. This work was supported by the National Natural Science Foundation of China (Grants No. 11974080, No. 11934014, No. 11704076, and No. U1732140). This work was partially supported by JSPS KAKENHI Grant No. JP19H00665.

- [1] M. C. Li, R. Si, T. Brage, R. Hutton, and Y. M. Zou, *Phys. Rev. A* **98**, 020502(R) (2018).
- [2] D. Layzer, *Ann. Phys. (NY)* **8**, 271 (1959).
- [3] D. Layzer and J. Bahcall, *Ann. Phys. (NY)* **17**, 177 (1962).
- [4] P. Jönsson, G. Gaigalas, J. Bieroń, C. Froese Fischer, and I. P. Grant, *Comput. Phys. Commun.* **184**, 2197 (2013).
- [5] J. A. Lowe, C. T. Chantler, and I. P. Grant, *Radiat. Phys. Chem.* **85**, 118 (2013).
- [6] T. A. Welton, *Phys. Rev.* **74**, 1157 (1948).
- [7] V. M. Shabaev, I. I. Tupitsyn, and V. A. Yerokhin, *Comput. Phys. Commun.* **189**, 175 (2015).
- [8] V. M. Shabaev, I. I. Tupitsyn, and V. A. Yerokhin, *Phys. Rev. A* **88**, 012513 (2013).
- [9] A. V. Volotka, M. Bilal, R. Beerwerth, X. Ma, Th. Stöhlker, and S. Fritzsche, *Phys. Rev. A* **100**, 010502(R) (2019).
- [10] V. M. Shabaev, I. I. Tupitsyn, M. Y. Kaygorodov, Y. S. Kozhedub, A. V. Malyshev, and D. V. Mironova, *Phys. Rev. A* **101**, 052502 (2020).
- [11] A. E. Kramida and G. Nave, *Eur. Phys. J. D* **39**, 331 (2006).
- [12] I. Draganić, J. R. Crespo López-Urrutia, R. DuBois, S. Fritzsche, V. M. Shabaev, R. S. Orts, I. I. Tupitsyn, Y. Zou, and J. Ullrich, *Phys. Rev. Lett.* **91**, 183001 (2003).
- [13] H. Feuchtgruber, D. Lutz, D. A. Beintema, E. A. Valentijn, O. H. Bauer, D. R. Boxhoorn, Th. De Graauw, L. N. Haser, G. Haerendel, A. M. Heras *et al.*, *Astrophys. J.* **487**, 962 (1997).
- [14] H. A. Robinson, *Phys. Rev.* **52**, 724 (1937).
- [15] K. E. Kissell and P. L. Byard, in *Proceedings of the 1965 Solar Eclipse Symposium* (NASA-Ames Research Center, Moffett Field, CA, 1965), p. 359.
- [16] W. C. Martin, R. Zalubas, and A. Musgrove, *J. Phys. Chem. Ref. Data* **19**, 821 (1990).

- [17] J. T. Jefferies, *Mem. Soc. R. Sci. Liege* **17**, 213 (1969).
- [18] V. Kaufman, J. Sugar, and D. Cooper, *Phys. Scr.* **25**, 623 (1982).
- [19] C. Jupén, *Phys. Scr.* **32**, 592 (1985).
- [20] B. Edlén, *Phys. Scr.* **26**, 71 (1982).
- [21] B. Edlén, *Phys. Scr.* **28**, 51 (1983).
- [22] B. Edlén, *Sol. Phys.* **9**, 439 (1969).
- [23] B. Edlén, *Opt. Pura Apl.* **10**, 123 (1977).
- [24] D. K. Nandy, *Phys. Rev. A* **94**, 052507 (2016).
- [25] B. Edlén, *Phys. Scr.* **8**, 5 (1984).
- [26] M. Eidelsberg, F. Crifo-Magnant, and C. J. Zeippen, *Astron. Astrophys. Suppl. Ser.* **43**, 455 (1981).
- [27] B. Edlén, *Z. Astrophys.* **22**, 30 (1943).
- [28] P. G. Judge, *Can. J. Phys.* **95**, 847 (2017).
- [29] W. Li, R. Casini, T. del Pino Alemán, and P. G. Judge, *Astrophys. J.* **848**, 82 (2017).
- [30] P. G. Judge, S. Habbal, and E. Landi, *Sol. Phys.* **288**, 467 (2013).
- [31] K. Lodders, [arXiv:1912.00844](https://arxiv.org/abs/1912.00844).
- [32] S. L. Keil, T. R. Rimmele, and J. Wagner, *Earth Moon Planets* **104**, 77 (2009).
- [33] R. Silwal, E. Takacs, J. M. Dreiling, J. D. Gillaspy, and Y. Ralchenko, *Atoms* **5**, 30 (2017).
- [34] J. Clementson, P. Beiersdorfer, G. V. Brown, M. F. Gu, H. Lundberg, Y. Podpaly, and E. Träbert, *Can. J. Phys.* **89**, 571 (2011).
- [35] P. Beiersdorfer, A. L. Osterheld, and S. R. Elliott, *Phys. Rev. A* **58**, 1944 (1998).
- [36] G. O’Neil, S. Sanders, P. Szypryt, Dipti, A. Gall, Y. Yang, S. M. Brewer, R. Doriese, J. Fowler, A. Naing, D. Swetz, J. Tan, J. Ullom, A. V. Volotka, E. Takacs, and Y. Ralchenko, *Phys. Rev. A* **102**, 032803 (2020).
- [37] W. Li, Y. Yang, B. Tu, J. Xiao, J. Grumer, T. Brage, T. Watanabe, R. Hutton, and Y. Zou, *Astrophys. J.* **826**, 219 (2016).
- [38] J. D. Gillaspy, T. Lin, L. Tedesco, J. N. Tan, J. M. Pomeroy, J. M. Laming, N. Brickhouse, G.-X. Chen, and E. Silver, *Astrophys. J.* **728**, 132 (2011).
- [39] N. Nakamura, E. Watanabe, H. A. Sakaue, D. Kato, I. Murakami, N. Yamamoto, H. Hara, and T. Watanabe, *Astrophys. J.* **739**, 17 (2011).
- [40] J. K. Lepson, P. Beiersdorfer, M. Bitter, and S. M. Kahn, *Can. J. Phys.* **86**, 175 (2008).
- [41] N. Nakamura, H. Kikuchi, H. A. Sakaue, and T. Watanabe, *Rev. Sci. Instrum.* **79**, 063104 (2008).
- [42] J. Xiao, R. Zhao, X. Jin, B. Tu, Y. Yang, D. Lu, R. Hutton, and Y. Zou, in *Proceedings of the 4th International Particle Accelerator Conference*, IPAC2013 (JACoW, Shanghai, China, 2013), pp. 434–436.
- [43] Q. Lu, J. He, H. Tian, M. Li, Y. Yang, K. Yao, C. Chen, J. Xiao, J. G. Li, B. Tu, and Y. Zou, *Phys. Rev. A* **99**, 042510 (2019).
- [44] A. Kramida, Yu. Ralchenko, and J. Reader, *NIST ASD Team, NIST Atomic Spectra Database*, Ver. 5.7.1 (National Institute of Standards and Technology, Gaithersburg, MD, 2019), <http://physics.nist.gov/asd>.
- [45] H. Ohashi, J. Yatsurugi, H. A. Sakaue, and N. Nakamura, *Rev. Sci. Instrum.* **82**, 083103 (2011).
- [46] L. J. Curtis and P. S. Ramanujam, *Phys. Rev. A* **26**, 3672 (1982).
- [47] E. R. Peck and K. Reeder, *J. Opt. Soc. Am.* **62**, 958 (1972).
- [48] Z. Shi, R. Zhao, W. Li, B. Tu, Y. Yang, J. Xiao, S. Huldt, R. Hutton, and Y. Zou, *Rev. Sci. Instrum.* **85**, 063110 (2014).
- [49] W. Li, Z. Shi, Y. Yang, J. Xiao, T. Brage, R. Hutton, and Y. Zou, *Phys. Rev. A* **91**, 062501 (2015).
- [50] See Supplemental Material at <http://link.aps.org/supplemental/10.1103/PhysRevA.98.020502> for different contributions to the fine structure of the $2p^5\ ^2P$ for ions in the F-like isoelectronic sequence.
- [51] M. C. Li, Ph.D. thesis, Fudan University, 2019.
- [52] Y.-K. Kim and K.-N. Huang, *Phys. Rev. A* **26**, 1984 (1982).
- [53] J. Hata, I. P. Grant, and B. P. Das, *J. Phys. B* **16**, L189 (1983).
- [54] P. Jönsson, A. Alkauskas, and G. Gaigalas, *At. Data Nucl. Data Tables* **99**, 431 (2013).
- [55] C. J. B. Pagan, G. H. Cavalcanti, C. Jupén, and A. G. Trigueiros, *Astrophys. J. Suppl. Ser.* **196**, 19 (2011).
- [56] P. Bengtsson, C. Jupén, L. Engström, A. Redfors, and M. Westerlind, *Phys. Scr.* **48**, 413 (1993).
- [57] E. Landi, G. Del Zanna, P. R. Young, K. P. Dere, and H. E. Mason, *Astrophys. J.* **744**, 99 (2012).
- [58] N. J. Peacock, M. F. Stamp, and J. D. Silver, *Phys. Scr.* **1984**, 10 (1984).